# CREVICE CORROSION DAMAGE ANALYSIS ON Ni-Cr-Mo ALLOYS PROPOSED FOR THE FABRICATION OF NUCLEAR WASTE CONTAINERS

P. Jakupi, D. Zagidulin, J.J. Noël, D.W. Shoesmith The University of Western Ontario, London, Ontario, Canada

#### **Abstract**

The crevice corrosion of Alloy-22 has been studied under constant applied current conditions in 5 mol/L NaCl at 120°C. Stable propagation could be achieved for applied currents of  $\geq 10~\mu A$ , but not for applied currents  $\leq 5~\mu A$ , despite a large number of initiation attempts. Initiation appears to require that the potential achieve a sufficiently positive value (200 mV vs. sat'd Ag/AgCl). Propagation occurs preferentially at the edge of the creviced area and spreads across, rather than penetrating into, the alloy surface. This may be due to the presence of a protective molybdenum gel layer on the exposed alloy surface.

#### 1. Introduction

Ni-Cr-Mo alloys were developed for their exceptional corrosion resistance in a variety of extreme corrosive environments<sup>1-7</sup>. We are studying the crevice corrosion of alloys in this series, in particular Alloy-22, since it is the reference material selected for the fabrication of nuclear waste containers in the Yucca Mountain repository (NV, USA). Therefore, it is necessary to assess how crevice corrosion may, or may not, propagate if the use of this alloy is to be justified. Consequently, our primary objective is the development of a crevice corrosion damage function that can be used to assess the evolution of material corrosion penetration rates.

### 2. Experimental

Crevice corrosion experiments were conducted using an electrochemical cell built within a Teflon-lined (polytetrafluoroethylene) Hastelloy pressure vessel<sup>8</sup>. A homemade Ag/AgCl (saturated KCl) reference electrode was used to measure the potential of the working electrode, and all potentials are quoted on this scale. Figure 1 shows a schematic of the v-shaped working electrode, counter electrode and reference electrode enclosed in the pressure vessel. The working electrode was machined and bent into a v-shape to ensure that only one crevice was formed in contact with the electrolyte solution. The crevice-forming face of the working electrode was polished with a series of wet silicon carbide papers (180, 320, 600, 800, 1000, 1200 grits). A small Teflon wafer was sandwiched between the flat metal surface of the working electrode and a polysulfone coupon to define the creviced area (approx. 4 cm<sup>2</sup>).

To prevent boiling of the electrolyte solution, the electrochemical cell was pressurized with 65 psi of ultra high purity argon gas. The temperature was controlled at  $120^{\circ}$ C in all experiments. During heat-up, the corrosion potential (E<sub>Corr</sub>) of the creviced

specimen was measured using a Solatron model 1284 potentiostat. All constant current experiments were performed using this same potentiostat.

After completion of each experiment, the creviced specimen was rinsed with deionized water and methanol and then dried. Various surface analytical techniques such as: Scanning Electron Microscopy (SEM) / Energy Dispersive X-ray analysis (EDX), Raman Spectroscopy, and Confocal Laser Scanning Microscopy (CLSM) were employed on the creviced area of the specimen to determine how the alloying elements of the alloy influence crevice corrosion.

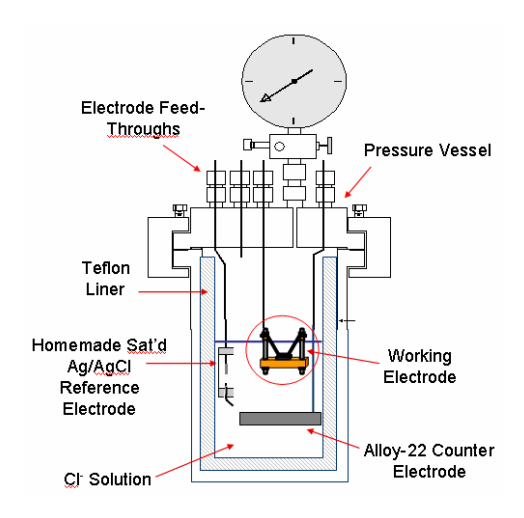


Figure 1: A schematic of the pressure vessel enclosing the electrochemical cell.

#### 3. Electrochemical Results

### 3.1 Crevice Corrosion Initiation and Propagation

All attempts to initiate crevice corrosion with the creviced electrode coupled to the counter electrode through the zero resistance ammeter were unsuccessful. Consequently, we resorted to initiating the process by applying a constant current. To determine the conditions for initiation, constant currents of various magnitudes were applied. Figures 2a and 2b show the crevice potentials ( $E_C$ ) measured at applied currents of  $200\mu A$  and  $10\mu A$ , respectively. The behaviour observed changed substantially with the value of the applied current.

At a current of 200  $\mu$ A,  $E_C$  increased rapidly to +480 mV before decreasing steadily to achieve a steady-state value of  $\sim$  -160 mV after  $\sim$  10 minutes, Figure 2a.  $E_C$  then remained constant at this value for the duration of the experiment. Such a positive potential excursion followed by a relaxation to a more negative value is characteristic of a transition from passive to active crevice behaviour. At the lower applied current of 10  $\mu$ A, figure 2b,  $E_C$  had the same form as at the higher current but was much noisier. At 10  $\mu$ A,  $E_C$  increased to a maximum value and eventually relaxed to a similar steady-state value of -160 mV. However, the transition from the passive to the active state was not so smooth. The noisy transient signals observed indicate a number of unsuccessful attempts

to initiate before an apparent success after  $\sim 10~000~s$  (compared to  $\sim 300~s$  (200  $\mu A$ )), when  $E_C$  decreased to a value of -100~mV. However, propagation was limited and repassivation occurred immediately after. Subsequently, after a further period of

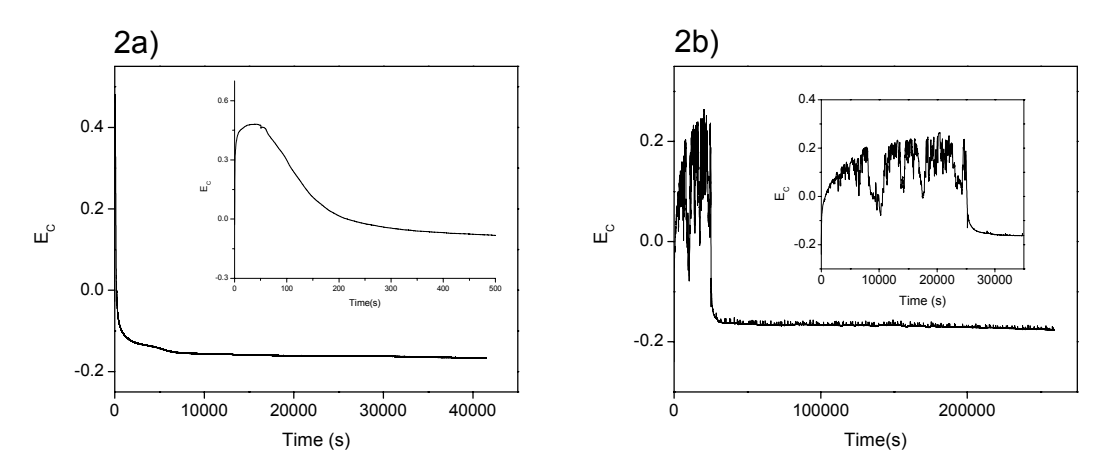


Figure 2: Galvanostatic initiation and propagation on Alloy-22 at applied currents (a)  $200 \mu A$  and (b)  $10 \mu A$ 

unsuccessful attempts, a second initiation occurred (at  $\sim$  26, 000 s) leading to stable propagation for over 3 days. The value of  $E_C$ , once propagation was underway, was the same as that achieved at 200  $\mu A$ .

## 3.2 Analyses of Crevice Corroded Surfaces

After completion of each crevice corrosion experiment, various surface analytical techniques were employed to investigate how the alloying components, Cr, Mo, and W, influence crevice corrosion initiation and propagation.

Optical micrographs of specimens crevice corroded with various applied currents showed that the damage spread laterally rather than into the alloy surface. For relatively lower applied currents the damage was not as wide spread as at higher applied currents. This trend is emphasized in the CLSM studies of the corroded specimens. SEM images reveal that grain boundary attack occurred and corrosion products were deposited on the bare grain surface. Raman analysis was performed on the regions where the corrosion products and grain boundary attack were observed. Figure 3 shows an optical micrograph of an attacked grain boundary and the corresponding Raman map. It is clear that the Raman signal intensity varies significantly between the attacked grain boundary and the un-attacked bare grain. Comparisons to literature spectra<sup>9,10</sup> reveal that the Raman signal is due to various molybdates specifically; MoO<sub>2</sub>, Mo<sub>4</sub>O<sub>11</sub> and NaMoO<sub>3</sub> · 3H<sub>2</sub>O. In the low pH environment characteristic of a solution confined within a creviced region, the dissolution of Mo<sup>n+</sup> and subsequent hydrolysis of these species eventually lead to the formation of insoluble molybdates that deposit within the attacked grain boundary regions and on adjacent bare grain surfaces.

Specimens corroded at different applied currents were also analyzed by CLSM to yield high resolution images and exact depth profiles of the crevice corroded regions. Figure 4 shows a CLSM image for an Alloy-22 specimen crevice corroded at an

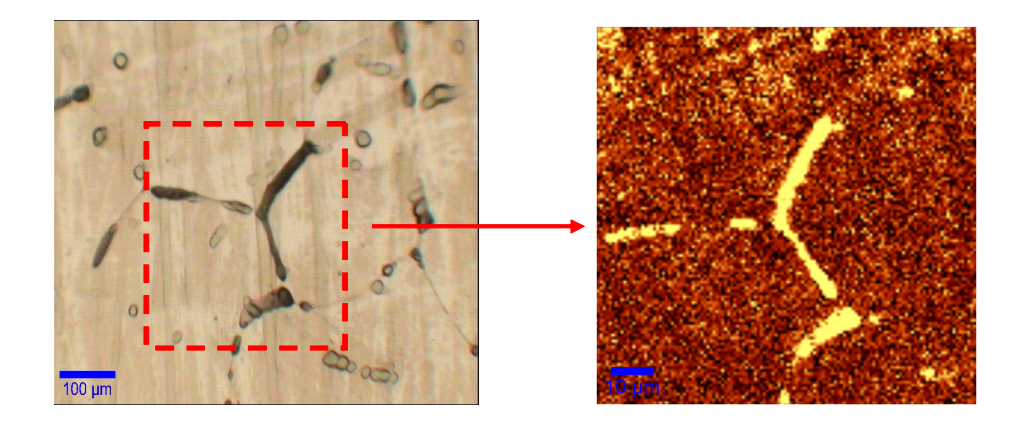


Figure 3: Optical micrograph of crevice corroded grain boundaries and the corresponding Raman signal intensity map.

applied current of 20  $\mu A$  and the corresponding depth profile from one end of the creviced region to the other end. The maximum depth of attack is shown to be  $\sim 25~\mu m$ . Scanning from the crevice mouth or edge of the creviced region towards the center of the damaged area a contrast in the morphology of attack was observed. Farthest from the crevice mouth grain boundary attack is dominant but near the crevice mouth crevice corrosion damage penetrates more deeply. It is found from the series of applied currents that the smaller the applied current the greater the penetration depth and the smaller the area corroded.

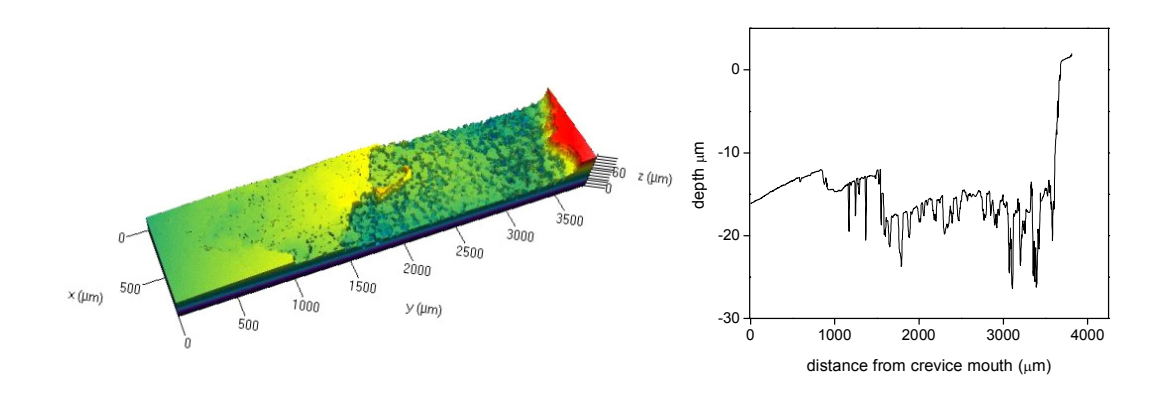


Figure 4: CLSM image for an Alloy-22 specimen crevice corroded at  $20\mu A$  and the corresponding line scan depth profile.

#### 4. Conclusions

A current threshold is necessary to initiate and subsequently propagate crevice corrosion on Alloy-22. Applied currents > 5  $\mu$ A crevice are required for corrosion initiation and propagation on Alloy-22.

During crevice corrosion insoluble molybdates are formed and cover the surface of the grains and accumulate in the attacked grain boundaries. These molybdates may inhibit metal dissolution on the grain surface and subsequent attempts to propagate in the grain boundaries may be inhibited for the same reason leaving only propagation across freshly exposed grains. This could account for the limited propagation into the material and the much more extensive propagation across the surface for specimens corroded at high currents.

### 5. Acknowledgements

Surface Science Western and Centre for Electrochemical Science and Engineering at University of Virginia.

Support of the Science and Technology Program of the Office of the Chief Scientist (OCS), Office of Civilian Radioactive Waste Management (OCRWM), U.S. Department of Energy (DOE) is gratefully acknowledged. The work was performed under the Corrosion and Materials Performance Cooperative, DOE Cooperative Agreement Number: DE-FC28-04RW12252.

The views, opinions, findings, and conclusions or recommendations of authors expressed herein do not necessarily state or reflect those of the DOE/OCRWM/OCS

### 6. References

- 1. G.M. Gordon, *Corrosion*, **58**, 811 (2002).
- D. S. Dunn, L. Yang, C. Wu, and G. A. Cragnolino, in *Scientific Basis for Nuclear Waste Management XXVIII/2004*, p. 33, Mat. Res. Soc. Symp. Proc. (2004).
- 3. S. D. Day, M. T. Whalen, K. J. King, G. A. Hust, L. L. Wong, J. C. Estill, and R. B. Rebak, *Corrosion*, **60**, 804 (2004).
- 4. D. D. Macdonald, G. Engelhardt, P. Jayaweera, N. Priyantha, and A. Davydov, *European Federation of Corrosion Publications*, **36**, 103 (2003).
- 5. B. A. Kehler, G. O. Ilevbare, and J. R. Scully, *Corrosion*, **57**, 1042 (2001).
- 6. K. J. Evans, A. Yilmaz, S. D. Day, L. L. Wong, J. C. Estill, and R. B. Rebak, *JOM*, **57**, 56 (2005).
- 7. D. S. Dunn, Y. M. Pan, K. T. Chiang, L. Yang, G. A. Cragnolino, and X. He, *JOM*, **57**, 49 (2005).
- 8. X. He, J.J. Noël, and D.W. Shoesmith, Corrosion Science, (2005), 47(5), 1177-1195.
- 9. S. Himeno, H. Niiya, and T. Ueda, Bull. Chem. Soc. Jpn., (1997), 70, 631-637
- 10. F. Hardcastle, I.E. Wachs, Journal of Raman Spectroscopy, (1995), 26, 397-405